

Evolution of SU(4) Transport Regimes in Carbon Nanotube Quantum Dots

A. Makarovski¹, J. Liu², and G. Finkelstein¹

Departments of ¹Physics and ²Chemistry, Duke University, Durham, NC 27708

Abstract

Carbon nanotubes present an ideal system for investigating electronic transport at the nanoscale. In this paper, we study the evolution of conductance regimes through nanotube Quantum Dot by controlling the contact transparency in high quality samples with doubly degenerate orbitals (“shells”). For sufficiently open contacts, Kondo behavior is observed for one, two, and three electrons in the topmost shell. As the contacts are opened even more, the sample enters the “Mixed Valence” regime, where different charge states are hybridized by electron tunneling. Here, the low-temperature conductance as a function of gate voltage shows pronounced modulations with a period of four electrons. The hallmark of the new regime is the lack of single-electron features at low temperature, which are uncovered when the temperature is raised. Finally, we find that for one and three electrons occupying a shell the zero-bias features behave distinctly differently in magnetic field.

At low temperatures, single-wall Carbon Nanotubes demonstrate a rich variety of transport regimes. In samples with low contact transparency, a pronounced Coulomb blockade [1] is observed, where single-electron conductance peaks are separated by broad “valleys” of vanishing conductance [2, 3]. A more complex behavior is revealed in samples with larger contact transparency, where the conductance is partially blockaded, but the signal in the valleys with a non-zero electron spin *increases* at low temperatures [4], manifesting the Kondo effect. This many-body effect, originally discussed in the context of bulk conductors [5] and resonant tunneling [6, 7] has recently been observed in a variety of systems, including semiconductor quantum dots [8-10], molecules [11, 12], carbon nanotubes [4, 13-15], and magnetic add atoms on metallic surfaces [16, 17].

The Anderson model of a localized magnetic impurity yields both the Kondo regime and the closely related Mixed Valence regime [18]. In the Kondo regime the charge of the system (impurity or nanostructure) is an integer while the spin state alternates. In the Mixed Valence regime the charge is not quantized and also fluctuates [5]. In the Coulomb Blockade systems, the Mixed Valence regime is usually realized in a narrow range of gate voltages close to the charge degeneracy points (*i.e.* in the vicinity of conductance peaks) [19]. However, if the

coupling to the contacts is increased, the regions of well-defined charge should gradually disappear and the Mixed Valence behavior should spread over the conductance valleys.

In this paper, we study the evolution from the Kondo to the Mixed Valence regime by controlling the contact transparency within the same semiconducting carbon nanotube sample. We work with high quality nanotubes, where the quantum-mechanical orbitals originating in two electronic subbands are doubly degenerate, forming four-electron “shells” [13-15, 20-25]. The Kondo effect in this situation is expected to obey the SU(4) symmetry [15, 26-29]. At low enough temperatures and sufficiently open contacts, the Kondo behavior develops in the valleys with one, two, and three electrons in the topmost shell [13, 14, 30]. As the contacts are opened even more, so that the individual charge states are no longer well defined, we observe the Mixed Valence behavior throughout the partially filled shell. In this regime, the four single-electron conduction peaks in a shell, visible at high temperature, merge at low temperatures into a single broad maximum. This temperature evolution is rather counterintuitive: the low temperature conductance does not display single electron features, which are uncovered only by *raising* the temperature. Finally, we study the conductance in the one, two and three-electron valleys in the Kondo regime as a function of magnetic field parallel to the nanotube axis. The zero-bias features in one and three-electron valleys, which appear identical at zero magnetic field, develop very differently as the field is applied.

The nanotubes were grown on a Si/SiO₂ substrate by Chemical Vapor Deposition using CO as a feedstock gas [31]. Cr/Au electrodes separated by 200 nm were deposited on top of the nanotubes. We chose ambipolar small-gap semiconducting nanotubes [32], with a high p-type conductance at negative gate voltages. At positive gate voltages, the middle section of the nanotube filled with electrons, which had to tunnel across the band gap to reach the contacts. Therefore, a quantum dot was formed between the tunneling junctions, and Coulomb blockade set in at low temperatures (Figure 1a). The single-electron conduction peaks cluster in groups of four, where each cluster corresponds to four electrons that fill a shell of two degenerate orbitals [13-15, 20-25]. Four such clusters, marked I-IV, are shown in Figure 1a.

The width of the tunneling junctions in our ambipolar nanotubes depends on the gate voltage: larger positive gate voltages make the junctions narrower (see schematics in Figure 1c) [33, 34]. Indeed, the peak widths grow as we increase the gate voltage in Figure 1a. Within each cluster, the peaks have a similar width. We therefore can vary the transparency of the contacts by changing the gate voltage. The extra control parameter allows us to study the evolution of transport regimes *within the same sample*.

The coupling to the contacts introduces a lifetime broadening Γ , which ranges from ~ 7 meV in cluster I to ~ 15 meV in cluster IV (as found from a multiple Lorentzian peak fit, see supplementary material). This broadening should be compared with other relevant energy parameters: the charging energy of $E_C \approx 10$ meV and the shell spacing of $\Delta \approx 10$ meV that we extract from Figure 1. The Kondo behavior should be observed in the valleys of clusters I and II, where $\Gamma < E_C$. However, in clusters III and IV, $\Gamma \geq E_C$; thus, the Mixed Valence regime should cover the entire cluster [35].

Indeed, in Figure 1a, clusters I and II demonstrate a conventional Kondo behavior: the single electron conduction peaks are well defined, and the signal in the valleys grows at lower temperatures. In particular, the Kondo behavior is observed in the two-electron valleys, indicating a degenerate ground state. The map of conductance as a function of the source-drain voltage V_{SD} and gate voltage V_{gate} (same range as in Figure 1a) is shown in Figure 1b. In the first four-electron cluster, the “Coulomb diamonds” are clearly visible. A ridge at zero source-drain voltage, typical for the Kondo effect [8, 9], forms across the three inner valleys of cluster I [14], and further grows in cluster II.

In clusters III and IV, the growth of conductance in the valleys completely washes away the single-electron peaks at the lowest temperatures. The unitary limit plateaus, observed for a well-developed Kondo effect at odd-integer fillings [36], are absent. Instead, we find deep oscillations with a periodicity of four electrons and the maximal conductance exceeding $2e^2/h$. Apparently, the maximum conductance is limited by $4e^2/h$, which is not reached due to asymmetry of the contacts. In the conductance map of Figure 1b, the zero-bias ridge becomes the most prominent feature.

In this sample, one of the contacts is more strongly coupled to the nanotube than the other, as evident from the lack of up-down symmetry in the image in Figure 1b. The weakly coupled contact may be viewed as a tunneling probe that senses the density of states in the nanotube strongly hybridized with the Fermi-sea of the other contact. The conductance is enhanced whenever the Fermi level of the weakly coupled contact is aligned with a resonance in the density of states of the nanotube. In the clusters III and IV, a single resonance descends from the positive source-drain

voltages to the Fermi energy as the gate voltage increases. The resonance dwells there (forming a zero-bias ridge), and then continues the descent to negative voltages.

For one electron, the SU(4) Kondo [26, 27] peak in the spectral density of states is expected to be shifted above the Fermi level by an energy of the order of $k_B T_K$ (*i.e.* by about its width) [29]. We can speculate that for three electrons (one hole) the resonance should move below the Fermi energy. For two electrons (two holes), the resonance should be centered at the Fermi energy. Indeed, as the number of electrons grows the resonances in clusters III and IV shift from just above zero to just below zero in V_{SD} . As a result the conductance ridge close to zero bias acquires a small, but noticeable, slope (Figure 1b).

The smooth conductance modulation with a period of four electrons, as observed at lowest temperatures in Figure 1a, is superficially similar to the single-particle (Fabri-Perot) interference [37]. Nevertheless, there are striking differences between the two regimes. First, the conductance map as a function of the source-drain and gate voltages in the single-particle regime demonstrates a crisscrossing grid of straight lines, corresponding to the (anti-) resonance interference conditions [37]. In our case, the conductance map is distinctly different: the positions (V_{SD} vs. V_{gate}) of the conductance resonances depend nonlinearly on the gate voltage (as discussed above; Figure 1b), indicating the importance of electronic interactions. Second, the temperature evolution of conductance in Figure 1a, indicates the presence of a new energy scale (~ 1 meV), which is significantly smaller than the single-particle energies (the shell spacing Δ and the charging energy E_C are both approximately equal to 10 meV). Third, the Fabri-Perot behavior is established for conductance oscillations, which have a small amplitude ($\sim 10\%$ of the background). We observe deep conductance variations between the centers of the four-electron clusters ($\sim 2e^2/h$) and the valleys between the clusters ($\sim 0.2e^2/h$). The direct application of the single-particle interference formula fails to adequately describe the conductance of clusters III and IV (dotted line in Figure 2a). The fit is uniquely fixed by the maximum to minimum ratio (~ 15 in experiment) and the gate voltage periodicity corresponding to adding four electrons per shell. Clearly the conductance maxima observed in our experiment are much wider than the result obtained from the single-particle formula.

We have successfully fitted the lowest temperature conductance for clusters III and IV by a remarkably simple formula: $G \sim \sin^2(\pi N/4)$ (Figure 2a). Here N (0 to 4) is the number of electrons on the topmost shell, which changes continuously with gate voltage $N = C_{gate}(V_{gate} - V_{gate}^{(0)})$. Although this functional form may seem deceptively simple, its implications are far reaching: Landauer’s formula predicts conductance in the form of $G = G_0 \sum_i \sin^2(\delta_i)$, where δ_i are the scattering phase shifts of different electron modes (enumerated by index i), traversing the

nanostructure [38]. In case of a nanotube, there are four modes ($i=1-4$), corresponding to two spin projections and two subbands. Friedel's sum rule [39], yields a relation between the number of electrons added to a nanostructure and the sum of the scattering phase shifts: $\sum_i \delta_i = \pi N$. If we assume that the scattering phases for all modes are equal to each other, we obtain $\delta_i = \pi N/4$. The conductance then becomes $G = 4G_0 \sin^2(\pi N/4)$, in accord with our observations.

We stress that $\delta_i = \pi N/4$ is by no means a trivial result: In the Kondo regime (no charge fluctuations), at low enough temperatures the scattering phase shifts of different modes are expected to become equal to each other [40]. This happens due to hybridization of the electron states in the Quantum Dot by electron tunneling to the contacts. For example, in the SU(4) case for one electron, $\delta_i = \pi/4$. In our case this result holds for a range of N , and not only for integer N as for the Kondo effect. Finally, the observed transport behavior is an essentially many-body effect. Indeed, the formula $G \sim \sin^2(\pi C_{\text{gate}}(V_{\text{gate}} - V_{\text{gate}}^{(0)})/4)$ works only at the lowest temperatures (where all δ_i become equal). The temperature evolution of the $G(V_{\text{gate}})$ curve, which reveals the single-electron features at higher temperatures, indicates that $\delta_i = \pi N/4$ breaks down already at $T \sim 5K$.

In Figure 2b we plot the conductance measured in the middle of the two-electron valleys (locations marked by symbols on Figure 2a) as a function of temperature. The high-temperature conductance for clusters III and IV and the low-temperature conductance for clusters I and II shows the logarithmic dependence expected for Kondo effect [35]. We have fitted the temperature dependence of conductance for clusters III and IV using the empirical formula of [19], used to fit the numerical Renormalization Group data of [41]. We find that the observed dependence is steeper than dictated by the original formula with an exponent of 0.22 and is visibly better described by an exponent of 0.25 for both clusters. The half-width of the Kondo ridge (2 meV) measured across the center of cluster IV (Figure 1b, $V_{\text{gate}} = 7.8$ V) agrees well with the characteristic temperature ($T_0 = 20$ K) extracted in Figure 2b. The relation between T_0 and other energy parameters is not precisely known in the SU(4) Mixed Valence regime; however, it seems surprising that T_0 is so much smaller than both Γ and E_C .

We now turn our attention to the SU(4) Kondo effect in the 1, 2, and 3-electron valleys at contact transparency such that the individual single-electron peaks are well-defined (as in clusters I and II of Figure 1a). In nanotubes, parallel magnetic field B_{\parallel} couples to both the spin and orbital magnetic moment of electrons [42]. The orbital magnetic moment μ corresponds to the electron motion around the nanotube circumference, and it is significantly larger than the spin magnetic moment μ_0 . Therefore, in magnetic field the levels in a four-electron cluster split into two doublets shifting higher or lower in energy with B_{\parallel} . Each doublet corresponds to two electrons

(spin-up and spin-down), occupying an orbital with a clockwise or counterclockwise direction of rotation with respect to magnetic field (Figure 3b). Figure 3a shows the nanotube conductance as a function of the gate voltage and magnetic field parallel to the nanotube axis. Three four-electron clusters are visible, which split into pairs of doublets, just as expected.

Figure 3c demonstrates conduction maps measured as a function of V_{SD} and V_{gate} at several B_{\parallel} . The Kondo ridge ($V_{SD} \approx 0$ at $B_{\parallel}=0$) visible in all three valleys (1e, 2e and 3e) splits at finite field in several arching horizontal lines at finite V_{SD} . The lines mark inelastic cotunneling thresholds; their appearance indicates that the ground state degeneracy is (partially) lifted. Such behavior is known as out-of-equilibrium Kondo effect [9, 43-46]. Let us consider the 2e valley first. At zero field, there are six different low-energy states of the two electrons in the nanotube (three different singlet states and one three-component triplet state, schematics in Figure 4b, [14]). The energy differences between these states, due to orbital mismatch, exchange interaction, and excess Coulomb interaction, are very small [24]. For a large enough lifetime broadening Γ , the states become effectively degenerate and can all participate in the formation of the Kondo resonance [47]. As B_{\parallel} is applied, a single state (the singlet with two electrons occupying the lower orbital) splits down from the rest. When the energy splitting becomes greater than the Kondo temperature ($\mu B_{\parallel} \sim k_B T_K$) at $\sim 1-2$ T, the zero-bias Kondo enhancement disappears (Figure 3a and c). It is replaced by the inelastic cotunneling thresholds which correspond to the excitation of the ground state (schematics in Figure 4e), and should appear at $eV_{SD} = \pm 2\mu B_{\parallel}$ (one of the two electrons is moved from the lower to the higher energy orbital in the shell).

The dependence of the co-tunneling features on magnetic field can be best traced in Figure 4, where we show the conductance measured as a function of V_{SD} and B_{\parallel} in the three valleys. In each field, the gate voltage is adjusted to stay in the centers of the 1e, 2e, or 3e valleys. For two electrons, the cotunneling thresholds indeed evolve linearly with field (Figure 4e) and can be used to estimate the electron angular momentum as $\mu=7\hbar$ and the diameter of the nanotube as $2nm$ [22, 42].

In addition to the excitations at $\pm 2\mu B_{\parallel}$, the 1e and 3e valleys also demonstrate lower energy features: two cotunneling lines at $eV_{SD} \sim \pm g\mu_0 B_{\parallel}$ in the 1e valley (Figure 4a, d) and a zero-bias peak in the 3e valley (Figure 4c, f). In both valleys, after the orbitals in the shell are split by more than the SU(4) Kondo temperature $T_K^{SU(4)}$, there is one electron left unpaired (on the lower or the higher orbital, respectively). This electron can form the SU(2) Kondo state as long as $g\mu_0 B_{\parallel} < k_B T_K^{SU(2)}$. Apparently this scenario is realized in the 3e valley. If the SU(2) Kondo temperature is less than $g\mu_0 B_{\parallel}$, the SU(2) Kondo state is not formed and cotunneling features at $eV_{SD} \sim \pm g\mu_0 B_{\parallel}$ should appear, as seen in the 1e valley. A similar 1e behavior was recently

observed [15] and attributed to the SU(4) Kondo effect [29].

We observe the difference between the 1e and 3e behaviors in several samples, and therefore it seems generic. It was also found in successive shells, so monotonic increase of Γ , and hence $T_K^{SU(2)}$ with V_{gate} may be ruled out. At present, it is not clear what is causing the difference in $T_K^{SU(2)}$ between the 1e and 3e valleys.

In conclusion, we study the evolution of conductance in a nanotube Quantum Dot with doubly degenerate orbitals as a function of the contact transparency. We identify the new transport regime, where the low temperature conductance shows no single electron features, which counterintuitively appear at high temperatures. This Mixed Valence regime is different from the related Kondo regime by a stronger electron tunneling to the contacts, which smears the charge quantization in the Dot. We successfully account for the low-temperature conductance as a function of gate voltage and for the temperature dependence of conductance at select gate voltages in the new regime. At the same time, the temperature evolution of the conductance curve as a function of gate voltage and the emergence of single electron oscillations at elevated temperatures remain a challenge. Finally, we study the Kondo effects at the 1, 2, and 3e occupation of the topmost shell, which depend differently on magnetic field parallel to the nanotube axis.

Acknowledgements: We thank H. Baranger, A. Chang, L. Glazman, E. Novais, K. Matveev, M. Pustilnik, and D. Ullmo for valuable discussions and A. Zhukov for technical assistance. The work is supported by NSF DMR-0239748.

Figure captions

Figure 1:

a) Differential conductance of a 200nm nanotube as a function of the gate voltage, measured at several temperatures. The single-electron conductance peaks cluster in groups of four, corresponding to four electrons filling the pairs of degenerate orbitals (“shells”). Four such clusters are shown; the numbers in the left two clusters indicate the number of electrons filling the shell. Since the transparency of the contacts grows with the gate voltage, the single-electron peaks become broader on the right. The Kondo effect enhances the conductance in the valleys within each cluster at low temperatures. Eventually, the single-electron conductance peaks within the two clusters on the right merge to form smooth oscillations with a four-electron periodicity.

b) Differential conductance map of the same sample as a function of the gate voltage (horizontal axis) and the source-drain voltage (vertical axis) at $T=3.3$ K. The outlines of the Coulomb diamonds are visible, most clearly in cluster I. Inside the “diamonds” the electronic transport

is blocked and the number of electrons in the nanotube is fixed. Following along a horizontal line, the transitions between the diamonds correspond to the conductance peaks. (Figure 1a can be viewed as a horizontal cross-section of Figure 1b.) The Kondo ridge is visible at zero source-drain voltage in all three valleys. Going from cluster I to cluster IV, the Kondo ridge going across each cluster becomes the most prominent feature of the data.

Colormap: 0  2.25 e²/h

c). Schematics: Band structure of a semiconducting nanotube. In ambipolar semiconducting nanotubes, the width of the tunneling junctions (red dotted line) at the contacts (orange squares) is controlled by the gate voltage: larger positive gate voltages bend the conduction band (green) and make the junctions narrower. Therefore, the transparency of the contacts grows with the gate voltage.

d) Schematics: In these data one of the contacts is better coupled to the nanotube than the other, which results in up-down asymmetry of Figure 1b. One can consider the weakly coupled contact as a tunneling probe, which measures a density of states in the system made of the nanotube and the strongly coupled contact.

Figure 2:

a) Conductance of clusters III and IV as a function of gate voltage (solid black line) and two fits. Blue dash-dot line: Fabri-Perot expression. Green dashed line: $G \sim \sin^2(\pi C_{gate}(V_{gate} - V_{gate}^{(0)})/4)$.

b). Symbols: temperature dependence of the conductance in the two-electron valleys (centers of the clusters are marked by corresponding the symbols in Figure 1a, clusters I-IV, bottom to top). Lines: fit using the empirical function of Ref. [19] (dashed blue line) and similar fit with an exponent of 0.25 instead of 0.22 (solid black line).

Figure 3:

a) Differential conductance as a function of V_{gate} and magnetic field parallel to the nanotube measured at $T=2.0$ K. The degenerate orbitals in a shell split as the magnetic field is applied, and move up or down in magnetic field depending on their chirality (clockwise or counterclockwise direction of rotation in field). Each orbital may be occupied by two electrons (triangle symbols pointing up or down). Therefore, within each cluster two lower (higher) single-electron traces move down (up) in magnetic field, denoted by empty (filled) symbols. At zero field, the signal between the peaks within each four-electron cluster is enhanced by the Kondo effect. This enhancement is suppressed by magnetic field (most effectively in the two-electron valley).

Colormap: 0  1.3 e²/h

b) Magnetic field parallel to the nanotube splits the four levels in a shell in doublets. Each doublet corresponds

to spin-up and spin-down electrons filling an orbital with a certain direction of rotation in magnetic field.

c) Differential conductance maps as a function V_{gate} and V_{SD} at several magnetic fields. At zero field, the Kondo ridge is visible in all three valleys. Orbital features split off (best visible in the 2e valley). At higher fields (4T and 6T), the 1e valley demonstrates two Zeeman-split features around zero-bias, while the 3e valley shows a single feature at zero bias.

Colormap: $0.1 \text{ e}^2/\text{h}$  $1.0 \text{ e}^2/\text{h}$

Figure 4:

Magnetic field behavior in the 1e, 2e and 3e valleys (left two right):

Main panel (a, b, and c): Differential conductance as a function of the V_{SD} at $T = 2.0 \text{ K}$ and different B_{\parallel} in the 1e, 2e and 3e valleys. B_{\parallel} ranges from 0 T to 9 T in 0.25 T increments (top to bottom). The curves are offset by 0.05 e^2/h per 0.25 T starting from 9 T. The gate voltage was adjusted to stay in the center of a valley when the magnetic field was changed. Kondo zero-bias peak (visible at $V_{SD}=0$, $B_{\parallel}=0$) splits into four, two, and three features in the 1e, 2e and 3e valleys respectively.

Top row schematics: possible states of 1, 2 and 3 electrons in the shell, and the transitions induced between them by the tunneling processes.

Bottom row (d, e, and f): same data as in the main panel, presented as grayscale maps as a function of the V_{SD} and B_{\parallel} . The larger energy cotunneling peaks in all three images (marked by dashed lines; also the symmetric features at positive V_{SD}) correspond to the orbital splitting. In the 1e valley, the lower splitting energy feature (marked by a dotted line) corresponds to the Zeeman splitting.

Bottom row schematics: level occupation and the possible excitations. For one and three electrons, both intra-orbital (spin) and inter-orbital excitations are possible, while for two electrons, only the inter-orbital excitations exist.

References

1. L.P. Kouwenhoven, C.M. Marcus, P.L. McEuen, S. Tarucha, R.M. Westervelt and N.S. Wingreen, *Electron Transport in Quantum Dots*, in *Mesoscopic Electron Transport*, L.L. Sohn, L.P. Kouwenhoven and G. Schon, Editors. 1997, Kluwer Academic: Boston. p. 105-214.
2. S.J. Tans, M.H. Devoret, H.J. Dai, A. Thess, R.E. Smalley, L.J. Geerligs and C. Dekker, *Individual single-wall carbon nanotubes as quantum wires*. *Nature* **386**, p. 474-477, (1997).
3. M. Bockrath, D.H. Cobden, P.L. McEuen, N.G. Chopra, A. Zettl, A. Thess and R.E. Smalley, *Single-electron transport in ropes of carbon nanotubes*. *Science* **275**, p. 1922-1925, (1997).
4. J. Nygård, D.H. Cobden and P.E. Lindelof, *Kondo physics in carbon nanotubes*. *Nature* **408**, p. 342-346, (2000).
5. A.C. Hewson, *The Kondo Problem to Heavy Fermions*. 1 Pbk ed. Cambridge Studies in Magnetism. 1997: Cambridge University Press.
6. L.I. Glazman and M.E. Raikh, *Resonant Kondo Transparency Of A Barrier With Quasilocal Impurity States*. *Jetp Letters* **47**, p. 452-455, (1988).
7. T.K. Ng and P.A. Lee, *On-Site Coulomb Repulsion And Resonant Tunneling*. *Physical Review Letters* **61**, p. 1768-1771, (1988).
8. D. Goldhaber-Gordon, H. Shtrikman, D. Mahalu, D. Abusch-Magder, U. Meirav and M.A. Kastner, *Kondo effect in a single-electron transistor*. *Nature* **391**, p. 156-159, (1998).
9. S.M. Cronenwett, T.H. Oosterkamp and L.P. Kouwenhoven, *A tunable Kondo effect in quantum dots*. *Science* **281**, p. 540-544, (1998).
10. J. Schmid, J. Weis, K. Eberl and K. von Klitzing, *A quantum dot in the limit of strong coupling to reservoirs*. *Physica B* **258**, p. 182-185, (1998).
11. J. Park, A.N. Pasupathy, J.I. Goldsmith, C. Chang, Y. Yaish, J.R. Petta, M. Rinkoski, J.P. Sethna, H.D. Abruna, P.L. McEuen and D.C. Ralph, *Coulomb blockade and the Kondo effect in single-atom transistors*. *Nature* **417**, p. 722-725, (2002).
12. W.J. Liang, M.P. Shores, M. Bockrath, J.R. Long and H. Park, *Kondo resonance in a single-molecule transistor*. *Nature* **417**, p. 725-729, (2002).
13. W.J. Liang, M. Bockrath and H. Park, *Shell filling and exchange coupling in metallic single-walled carbon nanotubes*. *Physical Review Letters* **88**, p. 126801, (2002).
14. B. Babic, T. Kontos and C. Schonenberger, *Kondo effect in carbon nanotubes at half filling*. *Physical Review B* **70**, p. 235419, (2004).
15. P. Jarillo-Herrero, J. Kong, H.S.J. van der Zant, C. Dekker, L.P. Kouwenhoven and S. De Franceschi, *Orbital Kondo effect in carbon nanotubes*. *Nature* **434**, p. 484-488, (2005).
16. V. Madhavan, W. Chen, T. Jamneala, M.F. Crommie and N.S. Wingreen, *Tunneling into a single magnetic atom: Spectroscopic evidence of the Kondo resonance*. *Science* **280**, p. 567-569, (1998).
17. J.T. Li, W.D. Schneider, R. Berndt and B. Delley, *Kondo scattering observed at a single magnetic impurity*. *Physical Review Letters* **80**, p. 2893-2896, (1998).
18. F.D.M. Haldane, *Scaling Theory Of Asymmetric Anderson Model*. *Physical Review Letters* **40**, p. 416-419, (1978).
19. D. Goldhaber-Gordon, J. Gores, M.A. Kastner, H. Shtrikman, D. Mahalu and U. Meirav, *From the Kondo regime to the mixed-valence regime in a single-electron transistor*. *Physical Review Letters* **81**, p. 5225-5228, (1998).
20. M.R. Buitelaar, A. Bachtold, T. Nussbaumer, M. Iqbal and C. Schonenberger, *Multiwall carbon nanotubes as quantum dots*. *Physical Review Letters* **88**, p. (2002).
21. S. Sapmaz, P. Jarillo-Herrero, J. Kong, C. Dekker, L.P. Kouwenhoven and H.S.J. van der Zant, *Electronic*

excitation spectrum of metallic carbon nanotubes. Physical Review B **71**, p. 153402, (2005).

22. P. Jarillo-Herrero, J. Kong, H.S.J. van der Zant, C. Dekker, L.P. Kouwenhoven and S. De Franceschi, *Electronic transport spectroscopy of carbon nanotubes in a magnetic field.* Physical Review Letters **94**, p. 156802, (2005).

23. S. Moriyama, T. Fuse, M. Suzuki, Y. Aoyagi and K. Ishibashi, *Four-electron shell structures and an interacting two-electron system in carbon-nanotube quantum dots.* Physical Review Letters **94**, p. 186806, (2005).

24. A. Makarovski, A. Zhukov, L. An, J. Liu and G. Finkelstein, *Persistent Orbital Degeneracy in Carbon Nanotubes.* cond-mat/0508401 (2005).

25. J. Cao, Q. Wang and H. Dai, *Electron transport in very clean, as-grown suspended carbon nanotubes.* Nature Materials **4**, p. 745-749, (2005).

26. G. Zarand, A. Brataas and D. Goldhaber-Gordon, *Kondo effect and spin filtering in triangular artificial atoms.* Solid State Communications **126**, p. 463-466, (2003).

27. L. Borda, G. Zarand, W. Hofstetter, B.I. Halperin and J. von Delft, *SU(4) Fermi liquid state and spin filtering in a double quantum dot system.* Physical Review Letters **90**, p. 026602, (2003).

28. K. Le Hur and P. Simon, *Smearing of charge fluctuations in a grain by spin-flip assisted tunneling.* Physical Review B **67**, p. (2003).

29. M.S. Choi, R. Lopez and R. Aguado, *SU(4) Kondo effect in carbon nanotubes.* Physical Review Letters **95**, p. 067204, (2005).

30. B. Babic and C. Schonberger, *Observation of Fano resonances in single-wall carbon nanotubes.* Physical Review B **70**, p. 195408, (2004).

31. B. Zheng, C.G. Lu, G. Gu, A. Makarovski, G. Finkelstein and J. Liu, *Efficient CVD growth of single-walled carbon nanotubes on surfaces using carbon monoxide precursor.* Nano Letters **2**, p. 895-898, (2002).

32. J. Cao, Q. Wang, M. Rolandi and H.J. Dai, *Aharonov-bohm interference and beating in single-walled carbon-nanotube interferometers.* Physical Review Letters **93**, p. 216803, (2004).

33. J.W. Park and P.L. McEuen, *Formation of a p-type quantum dot at the end of an n-type carbon nanotube.* Applied Physics Letters **79**, p. 1363-1365, (2001).

34. S. Heinze, J. Tersoff, R. Martel, V. Derycke, J. Appenzeller and P. Avouris, *Carbon nanotubes as Schottky barrier transistors.* Physical Review Letters **89**, p. (2002).

35. The transition between the Kondo and the Mixed Valence regimes is a crossover, rather than a Quantum Phase Transition. In the first case, $G \ll EC$ and the Kondo temperature is exponentially small; in the second case $G \sim EC$ and the effective temperature should be of the same order as G . Our association of Clusters I and II with a purely Kondo effect, and clusters III and IV with a purely Mixed Valence regime is a convenient approximation.

36. W.G. van der Wiel, S. De Franceschi, T. Fujisawa, J.M. Elzerman, S. Tarucha and L.P. Kouwenhoven, *The Kondo effect in the unitary limit.* Science **289**, p. 2105-2108, (2000).

37. W.J. Liang, M. Bockrath, D. Bozovic, J.H. Hafner, M. Tinkham and H. Park, *Fabry-Perot interference in a nanotube electron waveguide.* Nature **411**, p. 665-669, (2001).

38. M. Pustilnik and L. Glazman, *Kondo effect in quantum dots.* Journal of Physics-Condensed Matter **16**, p. R513-R537, (2004).

39. D.C. Langreth, *Friedel sum rule for Anderson's model of localized impurity states.* Physical Review **150**, p. 516-518, (1966).

40. P. Nozieres, *A "Fermi-Liquid" description of the Kondo problem at Low temperatures.* Journal of Low Temperature Physics **17**, p. 31-42, (1974).

41. T.A. Costi, A.C. Hewson and V. Zlatic, *Transport Coefficients Of The Anderson Model Via The Numerical Renormalization-Group.* Journal Of Physics-Condensed Matter **6**, p. 2519-2558, (1994).

42. E.D. Minot, Y. Yaish, V. Sazonova and P.L. McEuen, *Determination of electron orbital magnetic moments in carbon nanotubes.* Nature **428**, p. 536-539, (2004).

43. Y. Meir, N.S. Wingreen and P.A. Lee, *Low-Temperature Transport Through A Quantum Dot - The Anderson Model Out Of Equilibrium.* Physical Review Letters **70**, p. 2601-2604, (1993).

44. A. Kogan, S. Amasha, D. Goldhaber-Gordon, G. Granger, M.A. Kastner and H. Shtrikman, *Measurements of Kondo and spin splitting in single-electron transistors.* Physical Review Letters **93**, p. 166602, (2004).

45. D.M. Zumbuhl, C.M. Marcus, M.P. Hanson and A.C. Gossard, *Cotunneling spectroscopy in few-electron quantum dots.* Physical Review Letters **93**, p. 256801, (2004).

46. J. Paaske, A. Rosch, P. Wolfle, C.M. Marcus and J. Nygård, *Non-equilibrium singlet-triplet Kondo effect in carbon nanotubes.* Nature Physics **2**, p. 460-464, (2006).

47. The Kondo state observed here in the two-electron valley is expected [48] to obey the SU(4) symmetry. It should be different from the previously observed [49] two-electron singlet-triplet Kondo effect [50], where only four (and not six) degenerate states participate in the Kondo processes.

48. M.R. Galpin, D.E. Logan and H.R. Krishnamurthy, *Quantum phase transition in capacitively coupled double quantum dots.* Physical Review Letters **94**, p. 186406, (2005).

49. S. Sasaki, S. De Franceschi, J.M. Elzerman, W.G. van der Wiel, M. Eto, S. Tarucha and L.P. Kouwenhoven, *Kondo effect in an integer-spin quantum dot.* Nature **405**, p. 764-767, (2000).

50. M. Pustilnik and L.I. Glazman, *Conduction through a quantum dot near a singlet-triplet transition.* Physical Review Letters **85**, p. 2993-2996, (2000).

Figure 1

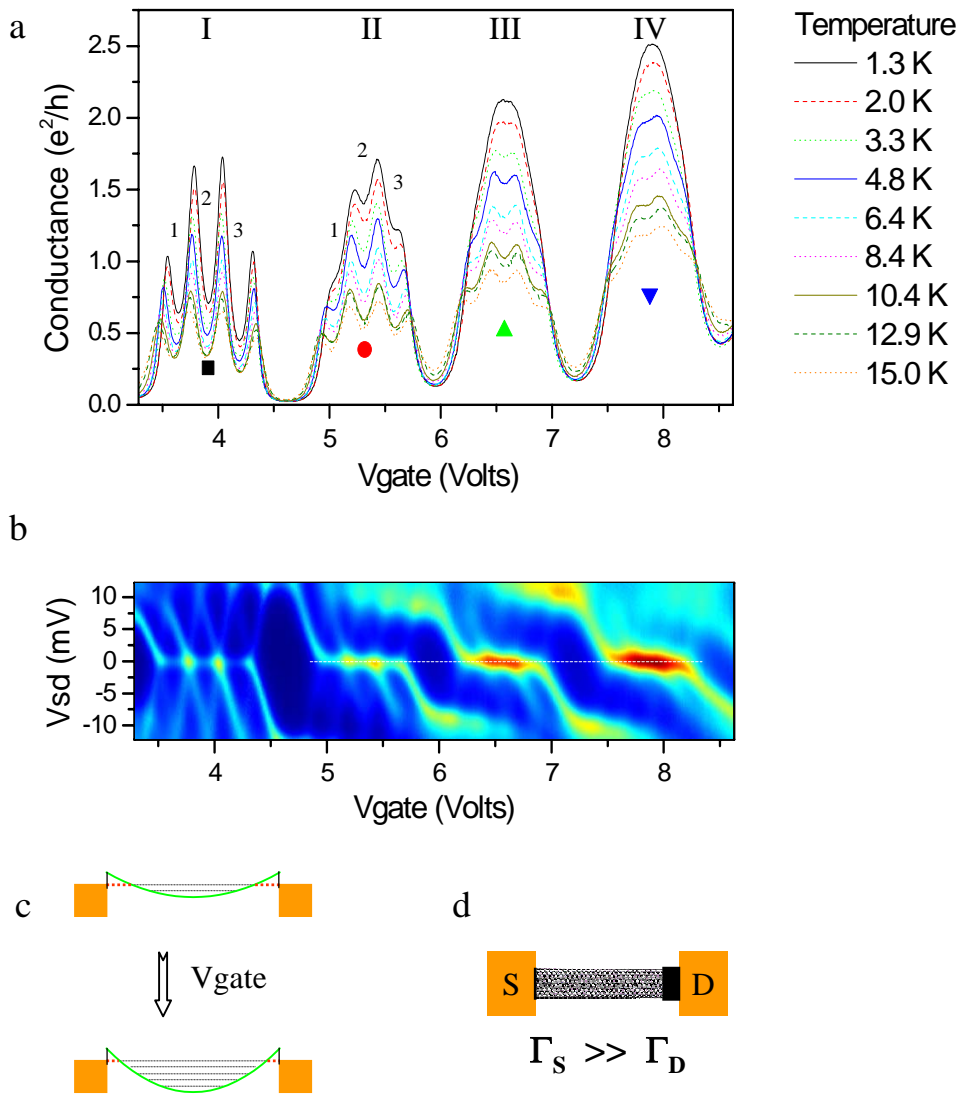


Figure 2

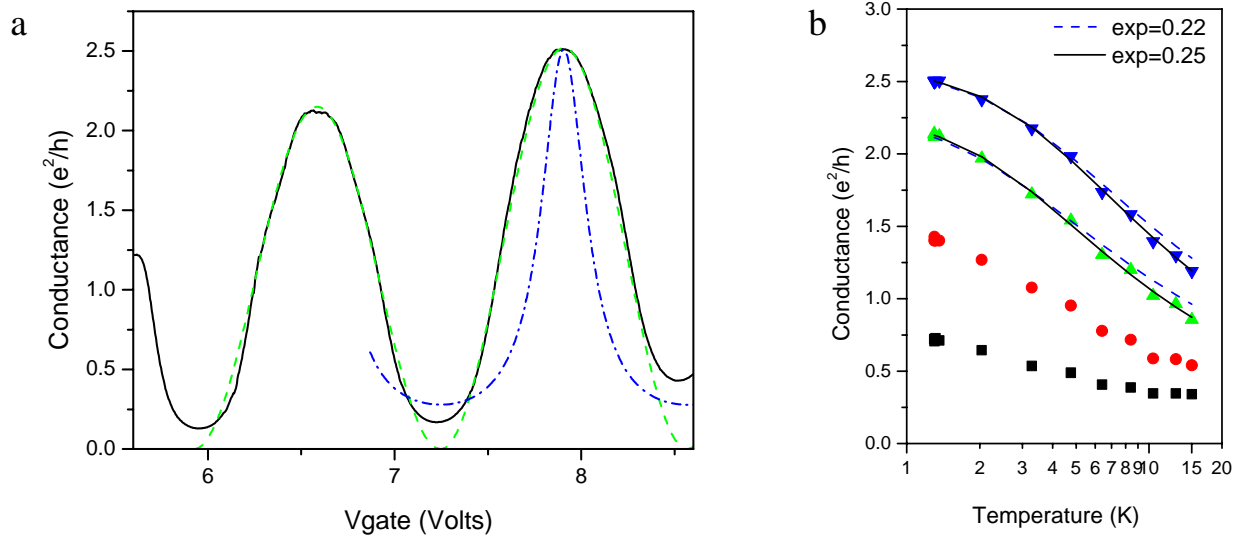


Figure 3

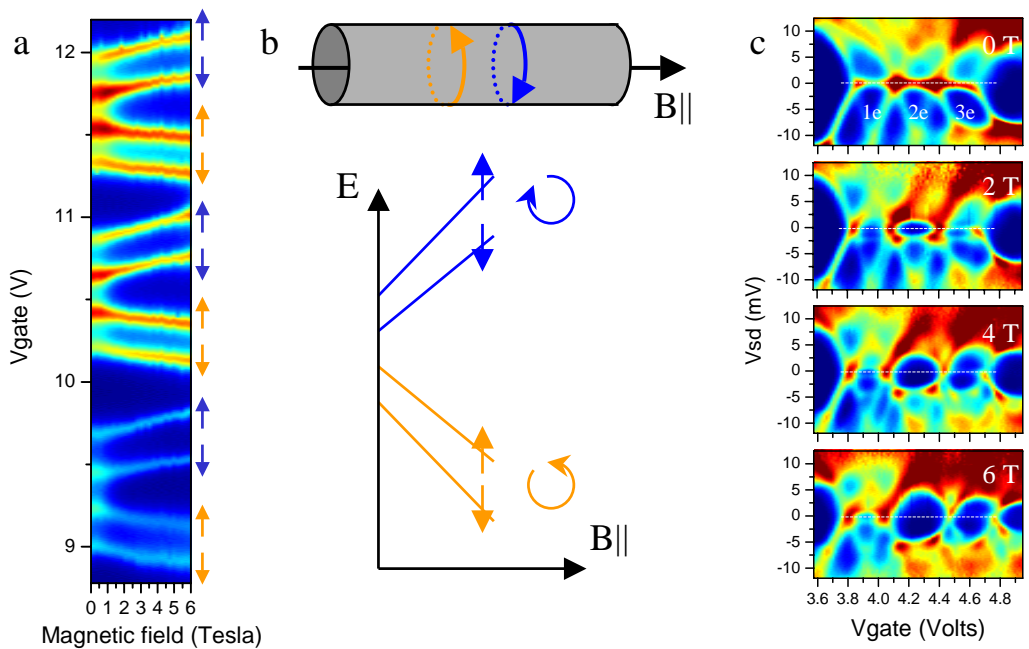
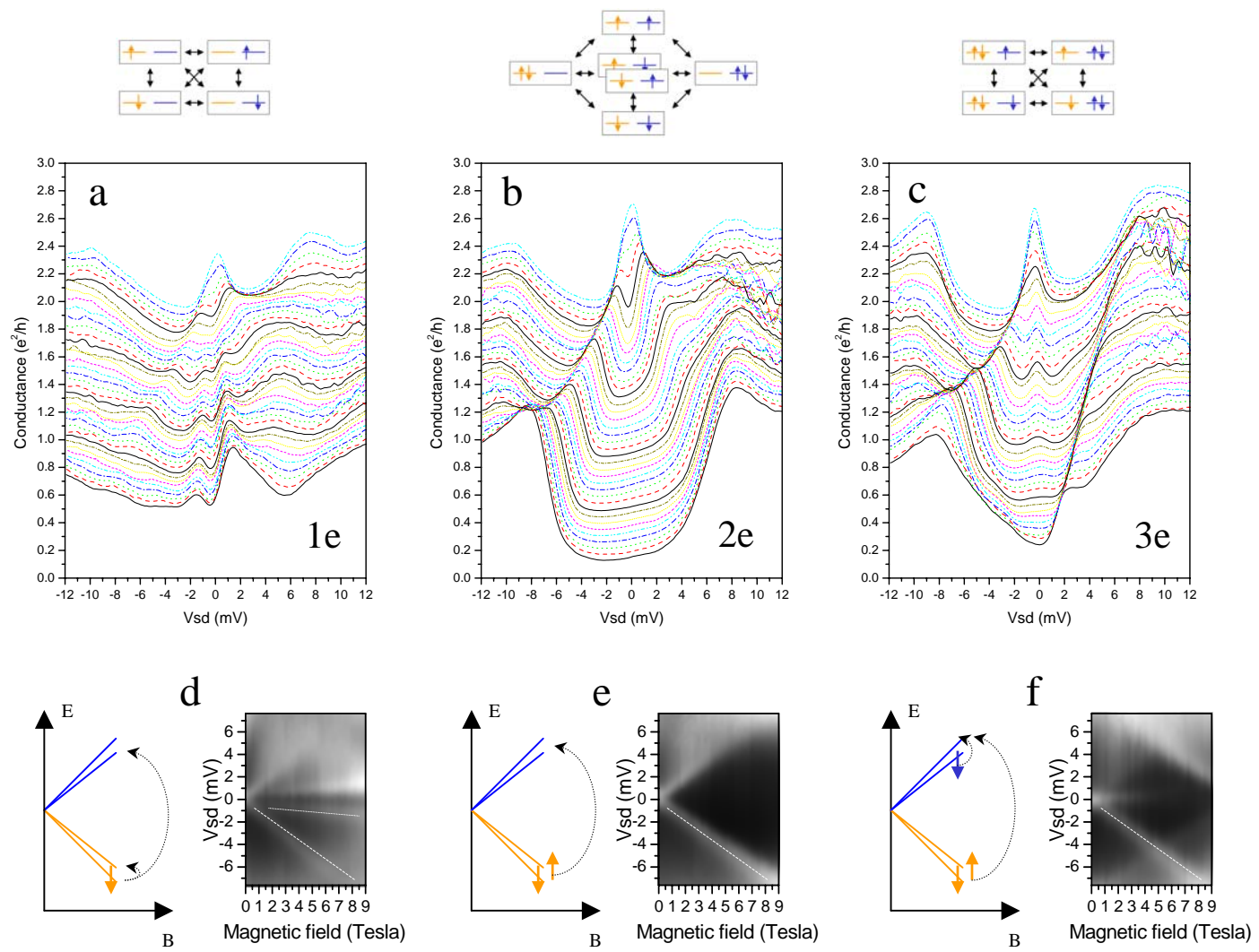


Figure 4



Supplementary information for:

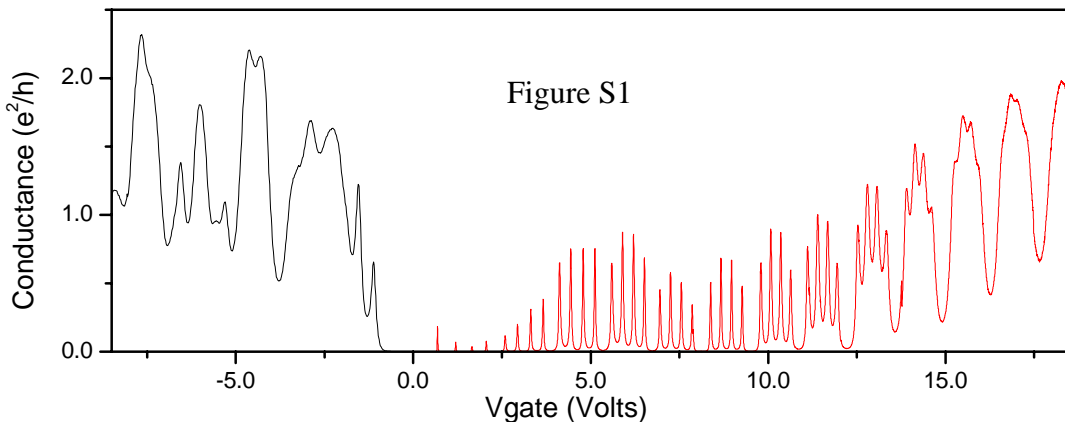
Evolution of SU(4) Transport Regimes in Carbon Nanotube Quantum Dots

A. Makarovski¹, J. Liu², and G. Finkelstein¹

Departments of Physics¹ and Chemistry², Duke University, Durham, NC 27708

Conductance overview.

We work with small gap semiconducting nanotubes. Cr/Au electrodes deposited on top of the nanotubes form high transparency p-type contacts. As a result, the samples demonstrate a relatively large conductance at negative gate voltages (Figure S1). At positive gate voltages, the n-type nanotube conductance is suppressed due to formation of the tunneling junctions at the contacts and Coulomb blockade oscillations set in. Clusters corresponding to four electrons filling a shell are clearly visible (red line).



Contact asymmetry and the maximal conductance.

From the nonlinear transport measurement of Figure 1b, we can estimate the ratio of the contact transparencies. The ratio of currents at positive and negative source-drain voltages when the shell is filled by zero or one electron is $(4\Gamma_S + \Gamma_D) / (\Gamma_S + 4\Gamma_D)$ [12]. Experimentally, in cluster IV this ratio is close to 2, which yields $\Gamma_S/\Gamma_D \sim 4$. We expect the maximal zero-bias conductance to be given by $G_{max} = 4e^2/h \cdot 4\Gamma_S\Gamma_D / (\Gamma_S + \Gamma_D)^2 \approx 2.5e^2/h$. This result is very close to the one found experimentally in Figure 1a.

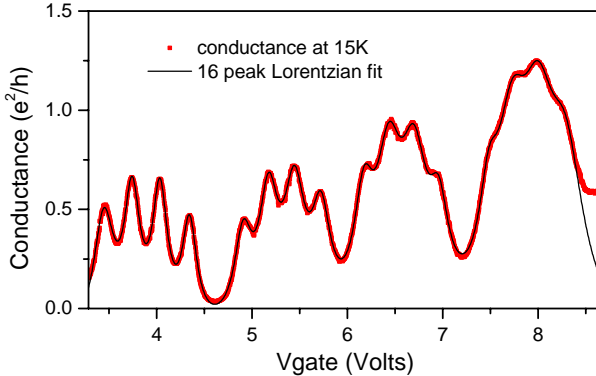


Figure S2

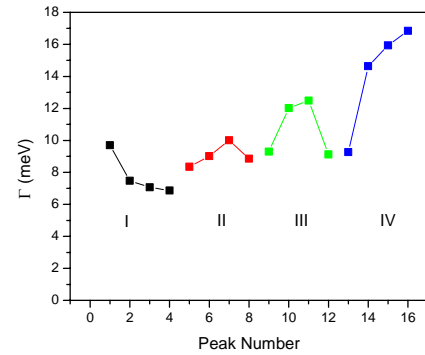


Figure S3

Fitting procedures.

1) In Figure 2a of the main text we used a 16-term Lorentzian to fit to the data measured at 15 K. The fitting parameters included the peaks heights, widths and positions, and an overall offset. Figure S2 demonstrates the quality of the fit and Figure S3 shows the lifetime broadening Γ that we deduced.

2) In Figure 2b we fit the temperature dependencies with the empirical formula of [18]: $G = G_0 [T' K^2 / (T' K^2 + T^2)]^s$. The first fit used the original exponent of $s=0.22$ and was optimized to fit the low temperature data points. This fit shows less pronounced temperature dependence at high temperatures than the actual data. The second fit uses s as a fit parameter. We find the optimal s of 0.25.

We have used Matlab Curve Fitting Toolbox for these fits.

Additional cotunneling features in B_{\parallel} .

We find that the odd-electron valleys also exhibit cotunneling features whose energy *decreases* with field. These features are best visible in Figure 4c, in which case the electron occupying the higher orbital of the partially filled shell can be excited to the lower orbital of the next, unoccupied shell. The energy of such an excitation is $\Delta E - 2\mu B$, where ΔE is the shell spacing at zero field. This energy becomes lower in magnetic field, as the corresponding levels come closer. Similarly, in a one-electron valley, an electron can be excited from a lower, completely filled shell, to the lower orbital of the partially filled shell, which is occupied by one electron. This process also requires an energy of

$\Delta E - 2\mu B$. In the case of a two-electron valley however, the inter-shell processes have energy of at least ΔE , so that no extra low-energy co-tunneling features are observed.

Energy levels in the 1e, 2e, and 3e valleys.

There are 4 degenerate states in the 1e valley (2 spins and 2 orbitals), resulting in SU(4) Kondo, as studied in [13]. The 3e valley should also have 4 degenerate states (the hole may occupy one of the 4 degenerate levels). In the 2e valley, there are 6 low-lying states (see schematics in Figure 4 and also [12]). These include the triplet state and 3 different singlet states. The energy differences between these states were experimentally studied by several groups [11, 12, 20-23]. We found these energy splitting negligible ($< 0.1 \Delta E$) in our samples [23]. Therefore, all the 6 closely spaced states are effectively degenerate and are involved in forming the Kondo state in the 2e valleys. In a number of papers (see *e.g.* [13]) some of the 6 states are split in energy. In our case, the states are degenerate at zero magnetic field, and the degeneracy is lifted when the field is applied. As a result, the Kondo enhancement is suppressed by magnetic field, and cotunneling features appear at finite V_{sd} proportional to magnetic field.